Coastal Engineering 113 (2016) 19–32

Contents lists available at ScienceDirect

Coastal Engineering

journal homepage: www.elsevier.com/locate/coastaleng

Sandbar and beach-face evolution on a prototype coarse sandy barrier

B.G. Ruessink [a,*], C. Blenkinsopp [b], J.A. Brinkkemper [a], B. Castelle [c,d], B. Dubarbier [c,d], F. Grasso [e], J.A. Puleo [f], T. Lanckriet [f,1]

[a] Institute for Marine and Atmospheric Research, Department of Physical Geography, Faculty of Geosciences, Utrecht University, P.O. Box 80.115, 3508 TC Utrecht, Netherlands
[b] Water, Environment and Infrastructure Resilience Research Unit, Department of Architecture and Civil Engineering, University of Bath, Bath BA2 7AY, United Kingdom
[c] CNRS, UMR EPOC 5805, 33615 Pessac, France
[d] Université de Bordeaux, UMR EPOC 5805, 33615 Pessac, France
[e] Ifremer — Dyneco/Physed, Centre Bretagne, BP70, 29280 Plouzané, France
[f] Center for Applied Coastal Research, Department of Civil and Environmental Engineering, University of Delaware, Newark, USA

ARTICLE INFO

Article history:
Received 23 February 2015
Received in revised form 5 October 2015
Accepted 10 November 2015
Available online 30 November 2015

Keywords:
Sandbar
Beach face
Surf–swash sand exchange
Swash dynamics

ABSTRACT

On steep beaches, the cross-shore movement of sand in response to 'erosive' storm waves and 'accretive' swell waves can lead to temporal changes between a barred winter profile and a non-barred summer profile with a pronounced berm in the upper swash zone. Despite recent improvements in predicting berm formation and evolution within process-based morphodynamic models, substantial demand for improvement in understanding swash processes and associated surf–swash sand exchange remains. Here, we analyze bed level data collected on a near-prototype, 4.5-m high and 75-m wide sandy beach (median grain diameter $D_{50} = 430$ μm) with a lagoon situated at its landward side. In particular, we distinguish between surf–swash sand exchange (time scale of tens of minutes to hours), the net effect of single and multiple swash events on the entire beach face (time scale of a few seconds to hours), and instantaneous bed variability at 3 cross-shore locations within individual swashes. During 'erosive' waves ($H_s = 0.8$ m, $T_p = 8$ s) sand on the initially 1:15 planar profile was predominantly eroded from the inner surf zone to be deposited in the outer surf zone as a sandbar, indicating minimal surf–swash sand exchange. Subsequent 'accretive' waves ($H_s = 0.6$ m, $T_p = 12$ s) caused substantially larger surf–swash sand exchange: the pre-existing sandbar migrated onshore and decayed, with the sand ending up on the beach face in a prominent (up to 0.7 m high), steep (1:6) berm. We found the dynamics of the berm to be governed primarily by wave conditions and the antecedent morphology, with ground water gradients of additional importance when morphodynamic feedback between swash flow and the berm is small. The observed bed level change within a swash and averaged over a swash event could be substantial (several centimeters) during all wave conditions, but the net (i.e., averaged over multiple swash events) bed level change was strongly suppressed because erosive and accretionary swashes nearly balanced. In addition, the local beach face slope could be instantaneously ≈ 25 % steeper or shallower than the median slope, or the initial or final slope. We anticipate that our data will stimulate new model development, as to increase the range of conditions and settings in which morphodynamic models can be applied realistically and reliably.

1. Introduction

The nearshore zone contains numerous morphological patterns, ranging from 0.1 to 1-m scale wave ripples to 100–1000-m scale sandbars (e.g., Holman, 2000). Temporal and spatial variability in sandbar position, including the formation and migration of rip channels, form the major source of nearshore bathymetric variability on the engineering time scale of weeks to years. Although sandbar dynamics can control the evolution of the beach face significantly (e.g., Sonu, 1973; Winant et al., 1975; Aubrey, 1979), sandbars are generally studied in isolation. This is, for example, illustrated by the inability of many process-based nearshore morphodynamic models (e.g., Plant et al., 2004; Ruessink et al., 2007; Kuriyama, 2012; Walstra et al., 2012; Dubarbier et al., 2015b) to handle swash processes and hence the exchange of sand between the barred surf zone and the beach. This represents a critical shortcoming of operational morphodynamic models, especially because many soft coastal protection measures, like sand nourishments (e.g., Hamm et al., 2002; Grunnet et al., 2004), are placed in relatively deep water under the assumption that natural processes, like waves and currents, will transport the sand onshore to result in wide beaches and strong dunes.

The volume of sand exchange between the barred surf zone and the beach face depends on the wave climate and beach type. In high-energy,

* Corresponding author. Tel.: +31 302532780; fax: +31 302531145.
E-mail address: b.g.ruessink@uu.nl (B.G. Ruessink).
[1] Now at International Marine & Dredging Consultants, Coveliersstraat 15, 2600 Antwerp, Belgium.

http://dx.doi.org/10.1016/j.coastaleng.2015.11.005
0378-3839/

gently sloping (say, < 1 : 30) nearshore zones with a typical median grain size of 200–300 μm and a tide range less than 4 m, the exchanged volume tends to be rather small compared to the total volume of sand typically present on the intertidal beach (e.g., Quartel et al., 2008). In this environmental setting, sandbars generally have multi-annual lifetimes, during which they rarely weld ashore, and near-bed sand fluxes in the trough separating the innermost sandbar from the beach are minimal irrespective of offshore wave conditions (e.g. Ruessink et al., 1998). In sharp contrast, the sand exchange on steeper, coarser grained beaches with a pronounced seasonality in the wave climate (high-energy, short-period storm waves alternating with low-energy, high-period swell waves) is substantially larger (e.g., Winant et al., 1975; Aubrey, 1979). Such beaches typically exhibit the transition between what has become known as a 'summer' and a 'winter' profile. Under the action of prolonged periods of 'summer' swell waves, pre-existing sandbars weld ashore to form a pronounced berm with a steep seaward flank and a more gently sloping landward side. This 'summer' profile is eroded during 'winter' storm waves, with the sand deposited in one or more sandbars. During the next 'summer' period, the sand is moved back onshore into a berm. Profile measurements reported in Aubrey (1979) show minimal bed level change around mean sea level, indicating that this position acts as the pivot point through which the sand is exchanged on a seasonal scale. The berm is formed by swash processes, causing the berm to grow vertically. Especially during high water levels (e.g., a high tide), the berm can be overtopped, causing a landward shift and rapid growth in sand volume due to a strong suppression of the backwash (Weir et al., 2006). Preliminary attempts to handle berm formation and evolution within process-based morphodynamic models are provided in Pender and Karunarathna (2013) and Kobayashi and Jung (2012), but substantial demand for improvement in understanding swash processes and associated surf–swash sand exchange remains (e.g., Puleo and Torres-Freyermuth, in press).

In 2012, the second large-scale Barrier Dynamics Experiment (BARDEX II), funded under the Hydralab IV program, was carried out in the Delta Flume, The Netherlands. The overall aim was to collect a near proto-type data set of energetic waves acting on a sandy beach/barrier system to improve our quantitative understanding and modelling capability of shallow water sediment transport processes in the inner surf, swash and overwash zone (Masselink et al., 2016). The third work package within BARDEX II focused on swash-surf exchange and sandbar dynamics, with the aims (1) to determine and quantify dominant hydrodynamic and sediment transport responsible for swash-surf zone sediment exchange and (2) to identify key processes responsible for onshore and offshore sandbar migration. The initial cross-shore profile of BARDEX II comprised a steep (1:15), coarse-grained barrier backed by a lagoon and was subject to 'erosive' winter waves and 'accretive' summer swell, and to different lagoon levels. The acquired data allowed us to explore surf–swash sand exchange (i.e., sandbar-berm dynamics) on the time scale of tens of minutes to hours, and beach face evolution from within a single swash to the net beach-face response of a single swash to a series of swash events (tens of minutes to hours), in response to different wave conditions and lagoon water levels (Sections 2 and 3). The latter were varied to promote conditions with both water infiltration and exfiltration through the beach face, allowing the effect on berm growth to be explored. We address the second aim with a recently developed, one-dimensional, phase-averaged morphodynamic model (Dubarbier et al., 2015b) that allows us to examine to what extent wave skewness, wave asymmetry, mean flow and gravity contributed to the sandbar dynamics observed during Bardex II (Section 4).

2. Methodology

2.1. BARDEX II

As part of BARDEX II (Masselink et al., 2016) a sandy barrier was constructed in the central region of the Delta Flume, Vollenhove, The Netherlands. The barrier, which filled the entire 5-m width of the flume, was composed of coarse ($D_{50} = 430$ μm; mean grain size = 510 μm), moderately sorted (0.81ϕ) and coarse-skewed (-0.24ϕ) quartz sand. The seaward part of the barrier profile initially comprised a 60-m long, 1:15 seaward-sloping section at cross-shore coordinates $x = 49 - 109$ m ($x = 0$ is at the wave paddle; Fig. 1a) between a 20-m long ($x = 29 - 49$m), 0.5-m thick sand bed and the 5-m long ($x = 109 - 114$ m), 4.5-m high horizontal barrier crest. The initial back-barrier profile comprised a 10-m long ($x = 114 - 124$ m), 1:5 landward-sloping section that ended at a 5-m high retaining wall. This permeable wall separated the back-barrier slope from a 10-m long lagoon at $x = 125 - 135$ m.

The Bardex II test program consisted of 19 distinct tests with different wave and water level conditions, grouped into 5 series that focused on surf–swash zone processes (series A–C), and barrier overwash and destruction (series D and E, respectively). Here, we analyze data collected during the 3 series that dealt with surf–swash zone processes; results for the barrier-overwash and destruction series can be found in Matias et al. (2016). In more detail, series A focused on beach response to varying wave conditions and different lagoon levels. Two different irregular wave conditions were used (see Table 1), expected to result in beach erosion (significant wave height $H_{s0} = 0.8$ m and peak period $T_{p0} = 8$ s; the subscript 0 signifies a value near the wave paddle) and accretion ($H_{s0} = 0.6$ m, $T_{p0} = 12$ s) with a sea level h_s of 3 m and low, intermediate and high lagoon levels of $h_l = 1.75$, 3, and 4.25 m, respectively (Table 1). Series B was designed to allow examination of sandbar dynamics in response to irregular erosive waves ($H_{s0} = 0.8$ m, $T_{p0} = 8$ s) and different sea levels ($h_s = 3$ and 2.5 m, respectively), see Table 1. Series C addressed tidal effects on beach profile development with irregular erosive wave conditions ($H_{s0} = 0.8$ m, $T_{p0} = 8$ s, with H_{s0} reduced to 0.6 m during the higher stages of the tide). The low-high-low tidal cycle was imposed as 30-min long segments of constant h_s, eventually making up a tidal range of 1.5 m and a period of 12 hours. During the rising tide (test C1) h_l was set to 1.75 m, while

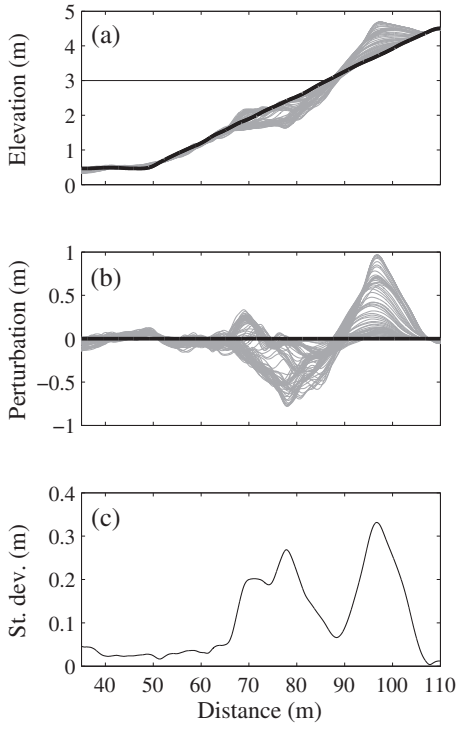

Fig. 1. (a) Elevation $z_{bb}(t)$, (b) perturbation $\tilde{z}_{bb}(t)$ and (c) standard deviation of $\tilde{z}_{bb}(t)$ versus cross-shore distance x for series A, B and C. (a) and (b) show 86 profiles in total. The thick solid line in (a) and (b) represents the initial profile. The horizontal solid line in (a) is the default sea level ($h_s = 3$ m).

Table 1
Experimental conditions of series A, B and C. H_{s0} = significant wave height; T_{p0} = peak wave period; h_s = sea level; h_l = lagoon level; T_{test} = test duration; and N_p = number of profiles.

Test	H_{s0} (m)	T_{p0} (s)	h_s (m)	h_l (m)	T_{test}(min)	cum. T_{test} (min)	N_p
A1	0.8	8	3	3–3.4	320	320	15
A2	0.8	8	3	4.3	200	520	6
A3	0.8	8	3	4.3	197	717	2
A4	0.8	8	3	1.75	200	917	6
A6	0.6	12	3	3	335	1252	14
A7	0.6	12	3	4.25	213	1465	6
A8	0.6	12	3	1.75	200	1665	6
B1	0.8	8	3	1.75	165	1830	5
B2	0.8	8	2.5	1.75	255	2085	6
C1	0.8, 0.6	8	2.25 → 3.65	1.75	330	2415	11
C2	0.8, 0.6	8	3.53 → 2.25	4.25	270	2685	9

during the falling tide (test C2) $h_l = 4.25$ m was used (Table 1). During all tests the irregular waves were constructed from a JONSWAP spectrum using the indicated H_{s0} and T_{p0} with a peak-enhancement factor of 3.3. The final ≈ 20 minutes of all tests in series A, however, comprised mono-chromatic and/or bi-chromatic waves. Their wave heights were selected such that the wave energy was the same as for the irregular wave conditions. The final 17 minutes of A3 are labeled as A5 in Masselink et al. (2016); no irregular wave runs were performed during A5 and, accordingly, this test is not mentioned separately in Table 1. The Automated Reflection Compensator was always switched on to avoid seiching in the flume.

2.2. Sandbar-berm bedlevel variability

Each test was generally broken up in several wave runs (Table 1) that varied in duration from 10 minutes to 3 hours. After each wave run, the center profile of the flume was surveyed using a profiling wheel mounted on an overhead gantry. Together with the initial profile, this resulted in 86 cross-shore profiles $z(x, t)$ (Table 1) with a 0.01-m cross-shore resolution; here, z is the elevation above the concrete floor of the flume, x is cross-shore distance and t is time. Each $z(x)$ profile was low-pass filtered using a second-order loess interpolator (Plant et al., 2002) with a cross-shore scale parameter l_x of 0.2 m to remove occasional spikes in the bed profile induced by glitches in the profiling system. Note that the second-order loess interpolator removes variability with length scales less than $l_x/0.7$. Visual inspection of $z(x, t)$ confirmed that the use of $l_x = 0.2$ m did not affect the height and length of omnipresent wave ripples; in the following $z(x, t)$ denotes the despiked data set of bed elevation. To separate large-scale morphological features, such as a sandbar and a berm, from the smaller-scale wave ripples, $z(x, t)$ was low-pass filtered with $l_x = 3.5$ m. The low-pass filtered data set contains these large-scale features and is denoted $z_{bb}(x, t)$. Finally, the initial profile $z_{bb}(x, t = 0)$ was subtracted from all $z_{bb}(x, t)$ to yield the perturbation data set $\tilde{z}_{bb}(x, t)$; positive and negative $\tilde{z}_{bb}(x, t)$ refer to bed elevations above and below $\tilde{z}_{bb}(x, t = 0)$, respectively.

Fig. 1 shows all $z_{bb}(x)$ and $\tilde{z}_{bb}(x)$ for series A, B and C, together with the standard deviation of $\tilde{z}_{bb}(x)$ of these 3 series. Bed level variability was most pronounced in the $x = 65 - 109$ m range, with an apparent nodal point at $x = 88$ m. Variability between $x = 65$ and 88 m was induced primarily by sandbar-trough dynamics (generation, migration, decay), while that between 88 and 109 m was caused by berm dynamics. Accordingly, the nodal point may be a pivot point (e.g., Aubrey, 1979) reflecting the exchange of sand between the sandbar and berm zone, but without any major local bed changes. To further quantify this exchange, the temporal evolution of the volume of sand per unit width was determined in the offshore region ($V_{off}(t), x = 31 - 65$ m), the sandbar-trough zone ($V_{bt}(t)$, $x = 65 - 88$ m) and the berm ($V_{berm}(t), x = 88 - 109$ m) using each $\tilde{z}_{bb}(x)$ and the trapezoidal rule.

Based on the continuity equation of sediment mass, the cross-shore volumetric transport rate, $q(x)$, with unit m^3/m/s between two surveys separated by time span dt was estimated as

$$q(x) = q_0 - (1-p)\int_{x0}^{x} \frac{dz_{bb}}{dt}\,dx, \quad (1)$$

where $p = 0.35$ is the porosity. Eq. (1) was solved in the seaward direction from the landward end of the berm zone, $x_0 = 109$ m, to the seaward start of the 1:15 slope, $x = 49$ m. Thus, dx is negative and shoreward transport is positive. The transport rate q_0 at x_0 was set to 0. Previous observations (e.g., Gallagher et al., 1998; Hoefel and Elgar, 2003) and modelling (e.g., Ruessink et al., 2007) has indicated that the sign of q is generally positive (onshore) when waves are non- to weakly breaking and negative (offshore) when wave breaking is more pronounced. Here, the cross-shore evolution of the fraction of breaking waves, $Q_b(x)$, was determined for each run from cross-shore time stacks of instantaneous (20 Hz) image intensity collected with three Argus-style (Holman and Stanley, 2007) video cameras. In these stacks breaking waves have substantially higher intensity than non-breaking waves, allowing both to be counted on a wave-by-wave basis and to estimate $Q_b(x)$, see Brinkkemper et al. (2016) for details.

2.3. Bedlevel variability in the swash zone

A single line of 45 Massa M300/95 ultrasonic altimeters (BLS) were mounted on a scaffold frame at a cross-shore spacing of 0.75 m to yield beach face elevation change and mass flux of sediment per swash event. The sensors (Turner et al., 2008) were mounted approximately 1 m above the beach face and were used to obtain measurements of the vertical distance to the nearest target: the sand surface when the bed was 'dry' and swash surface when the bed was submerged. The ultrasonic altimeter measurements were pre-processed to separate the dry bed and swash surface parts of the time-series for each sensor. Bed detection was achieved using the method used by Turner et al. (2008) and Blenkinsopp et al. (2011), where it is assumed that the bed is present when the rate of change of elevation is below a threshold value of 0.0005 m/s for a period of at least 1.5 s. Due to the small number of valid bed detections below the still water level (SWL), only those ultrasonic sensors between $x = 87.9$ m and $x = 108.9$ m from the wave paddle were used in the swash zone morphology analysis. Mass flux of sediment per swash event was calculated by integrating the change in beach face sediment mass landward of the point of interest as described by Blenkinsopp et al. (2011). The analysis focused on two erosive tests (A2 and A4) and two accretionary tests (A7 and A8). As each of these tests was split into separate runs, the runs were concatenated to enable an analysis of the swash zone morphology changes during the entire tests.

High-frequency (i.e., during a swash event) bed level oscillations were quantified using Conductivity Concentration Profilers (CCPs; see Lanckriet et al., 2013) and ultrasonic altimeter sensors located at $x = 88$, 89.5 and 91 m. CCPs measure the conductivity of the sediment-fluid matrix using an narrow array of 32 gold-plated electrodes separated by 1 mm in the vertical. At each cross-shore location at least 2 CCPs were deployed being separated in the alongshore direction by approximately 0.2 m. Sensors were deployed with the water proof housing buried into the bed with only the small measurement probe exposed. Adjacent sensors at a given cross-shore location were buried at slightly different depths (e.g. sensors are offset vertically) in an effort to increase the vertical sampling range. Raw CCP data were converted to volumetric sediment concentration using Archie's Law (Archie, 1942) and the packed bed and clear water conductivities (see Lanckriet et al., 2013). Sensor readings in air yield erroneous values due to low conductivity and are removed from the record. Each sediment concentration profile generally shows a transition from high values in the bed to lower values in the lower water column indicating

the bed level boundary. The bed level is defined based on the shoulder region of the concentration profile following O'Donoghue and Wright (2004) and Lanckriet et al. (2014). This definition for bed level is similar to that defined by the loose packing limit (Bagnold, 1966) at a volumetric concentration of 0.51.

The CCP profiling range of 0.03 m for an individual sensor means that the bed level will often reside outside the measurement window. Only data from tests A2 and A4 are shown here because the CCPs were either often buried or above the bed level during tests A7 and A8. Even for tests A2 and A4 data from the earlier runs when the beach was rapidly adjusting are too intermittent to yield consistent results. Thus, only data from the final 60 min with irregular wave action, when the beach was adjusting more slowly, are shown. During this time, multiple CCPs at a single cross-shore location often allowed for some overlapping of the profile range (Fig. 2). Corresponding bed levels from the altimeters are also shown. The elevation relative to the initial bed level indicates that the beach for test A2 underwent slight erosion at all three cross-shore locations. The altimeter and CCP data show similar trends. Gaps or lack of CCP data at the landward station are due to the bed level falling outside the measurement window as mentioned. Gaps in the altimeter data are due to the water depth not receding sufficiently to expose the bed. Data for test A4 indicate little net change over the run duration. Altimeter data are able to capture the bed level at the more landward locations when it falls outside the CCP measurement range. No CCP data were available at the landward location for test A4 but the altimeter data also show the bed level change little in a net sense.

3. Results: observations

3.1. Sandbar-berm dynamics

The erosive waves during tests A1–A4 reshaped the initially planar beach into a barred profile (Fig. 3a), with the sandbar (positive $\tilde{z}_{bb}$) between $x = 65$ and 73 m and the trough (negative $\tilde{z}_{bb}$ between 73 and 88 m, Fig. 3b). The sandbar formed at the location where approximately 15 to 20% of the waves broke on the initial profile (~ outer surf zone, see Fig. 3d). In contrast to the classic breakpoint hypothesis for sandbar generation, in which the sandbar forms because of convergence of onshore transport in the shoaling zone and offshore transport in the surf zone, the sandbar formed primarily because of a decline in offshore directed transport from the surf toward the shoaling zone (Fig. 3c). In Section 4 we discuss the importance of velocity skewness and asymmetry, mean currents and gravity to the observed transports using numerical modelling. As can also be deduced from Fig. 3c, the sandbar formed largely during the first 90 min of wave action. During the subsequent 350 minutes, the sandbar slowly grew in height (Fig. 3b), after which q was ≈ 0 over the sandbar region and the sandbar remained unchanged. On the whole, this suggests that the sandbar was more-or-less in equilibrium with the wave conditions after several hours of wave action. The sandbar-trough formation resulted from sand redistribution seaward of the pivot point (i.e., seaward of the still water position), as the change in V_{bt} with respect to the volume in the initial profile during tests A1–A4 is minor (Fig. 4a). Estimating volume changes for the sandbar ($x = 65 - 73$ m) and trough ($x = 73 - 88$ m) region

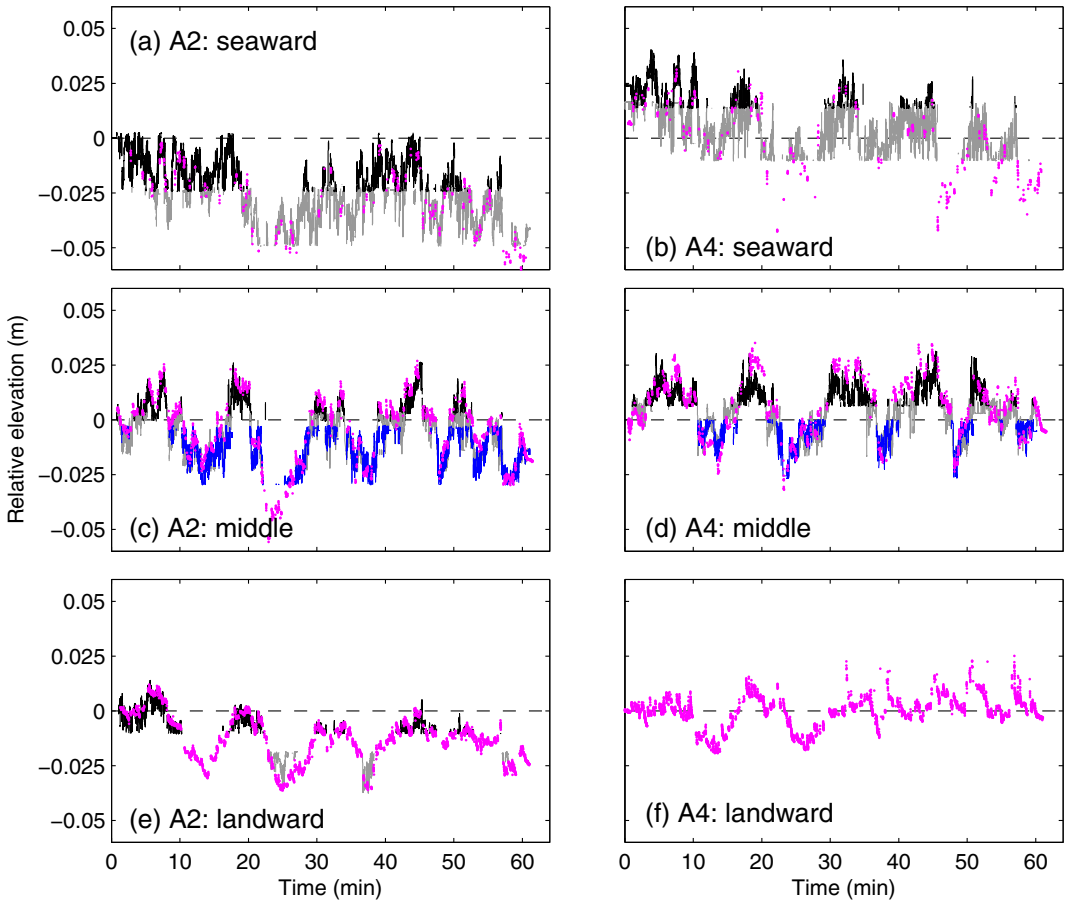

Fig. 2. CCP and BLS bed level elevation relative to the initial bed position. a), c), and e) Test A2 at the 3 cross-shore CCP location. b), d), and f) Test A4 at the 3 cross-shore CCP locations. CCP data shown in black, gray and blue when available from different sensors separated in the alongshore direction. BLS data shown as magenta filled circles when available.

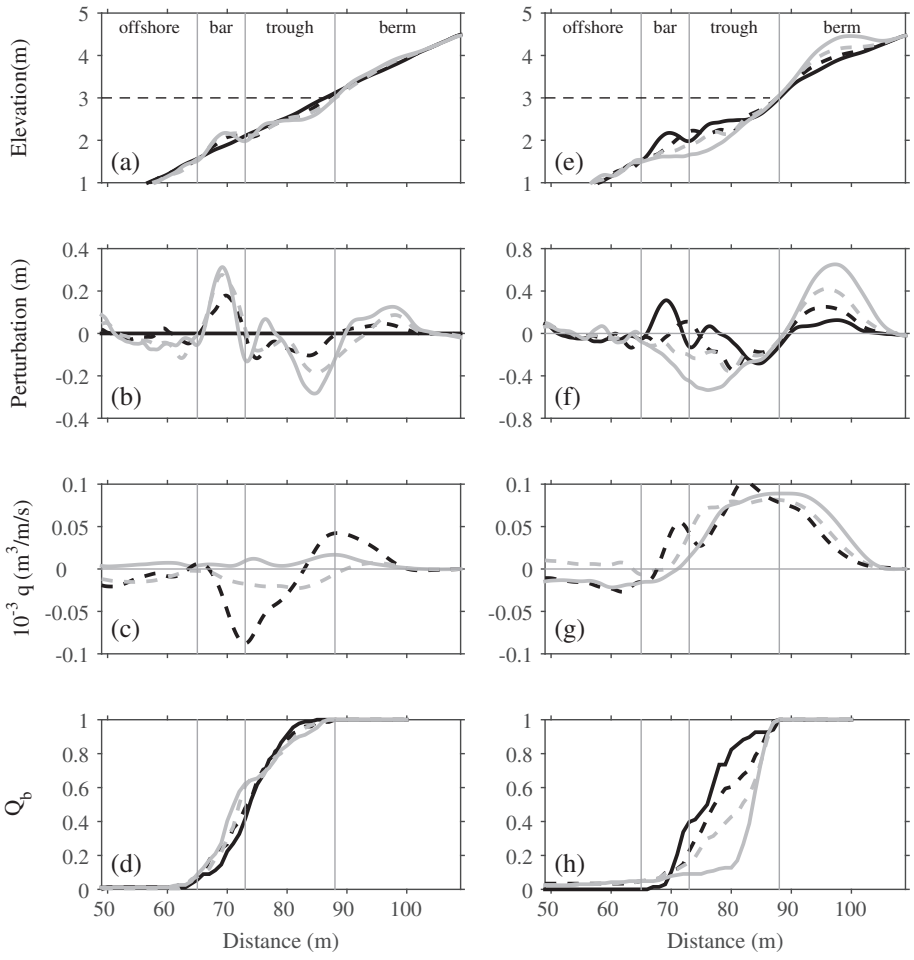

Fig. 3. (Top to bottom) Bed elevation z_{bb}, perturbation $\tilde{z}_{bb}$, volumetric transport rate q and fraction of breaking waves Q_b versus cross-shore distance x for the (left column) erosive wave tests A1–A4 and (right column) accretionary wave tests A6–A8. In (a), (b) and (d) the solid black line is time $t = 0$ (A1), the dashed black line $t = 90$ min (A1), the dashed gray line $t = 440$ min (A2) and the solid gray line $t = 917$ min (A4). In (c), the dashed black line is q with the profiles at $t = 0$ and 90 min, the dashed gray line with $t = 90$ and 440 min, and the solid gray line with $t = 440$ and 917 min. In (e)–(h) the order of the lines is the same as in (a)–(d), but now with $t = 917$ (A4), 1112 (A6), 1342 (A7) and 1665 min (A8). The horizontal dashed line in (a) and (e) indicates sea level h_s.

separately reveals a rapid increase in V_{bar} and a similarly rapid decrease in V_{trough} during the first 90 minutes of A1 (Fig. 4a). In more detail, V_{trough} exceeded V_{bar} slightly, causing a minor decline in V_{bt}. This sand was transported ashore (Fig. 3c) to form an approximately 0.1 m high berm in the upper swash zone (Fig. 4a–b). The volume change in the offshore zone ($x = 31 - 65$ m) was negligible during tests A1–A4 (Fig. 4b).

During tests A6–A8 the pre-existing sandbar-trough disappeared and was reshaped into a terrace-like feature, while at the same time a prominent berm formed at $x = 88 - 109$ m with its crest at $x = 97$ m, a steep (1:6) seaward side and a gently dipping profile on the landward side (Fig. 3e). After almost 12.5 hours of accretionary wave action, the berm had reached a height of almost 0.7 m (Fig. 3f) and a volume of about 7 m^3/m (Fig. 4a). Approximately the same amount of sand was lost from the sandbar-trough zone (Fig. 4a), implying this to be the main source of sediment and not, as was the case for tests A1–A4, the lower swash zone only. Interestingly, the increase in V_{berm} observed in tests A6–A8 was approximately linear with time (≈ 0.5 m^3/m/hour), indicating that equilibrium had not been reached at the end of A8. Also, we do not see any clear changes in the growth of V_{berm} in response to different lagoon levels (for example, h_l was 1.75 m during A8 and 4.3 m during A7), indicating that lagoon level did not affect the growth in V_{berm} for the conditions studied here (see Section 3.2). As seen in Fig. 3g, sand transport was onshore directed ($q > 0$) throughout the entire sandbar-trough and berm zone (i.e., including the surf zone), with a rather flat peak around the still water position. The small gradients in q explain the rather small bed level changes around this location, leading to the pivot point visible in Fig. 1c. The peak magnitude in q is about equal to that during the erosive waves in the outer surf zone when the sandbar formed (see Fig. 3c and g). As observed under the erosive waves, q was approximately zero in the offshore region (Fig. 3g). As the sandbar-trough disappeared, wave breaking became increasingly focused at the still water level, with an increase in Q_b from 10 to 100% over a less than 10-m wide region during A8 (Fig. 3h). Note that q remained large (and positive) in the former sandbar-trough region, even though the water depth increased by over 0.5 m and Q_b dropped to less than 10%.

During the erosive wave conditions of series B and C the sandbar and the berm remained relatively stable (Figs. 5a and d, and 4a). During these series, the sandbar response depended on the fraction of breaking waves, with, in general, onshore sandbar migration when $Q_b < 20$ % and offshore sandbar migration when wave breaking was more intense. The former case was observed during B1 and C, except for the runs with the lowest water levels. For example, as tests A6–A8 had resulted in a rather deep ($z \approx 1.7$ m, hence water depth $h \approx 1.3$ m during B1) flat terrace, only few waves broke here during test B1 ($Q_b < 20$ %, Fig. 5c) and the outer surf zone was wide. The sand transport was, compared to the longer-wave period conditions of tests A6–A8, rather low but still onshore directed (Fig. 5b) and the sandbar moved onshore to a crest

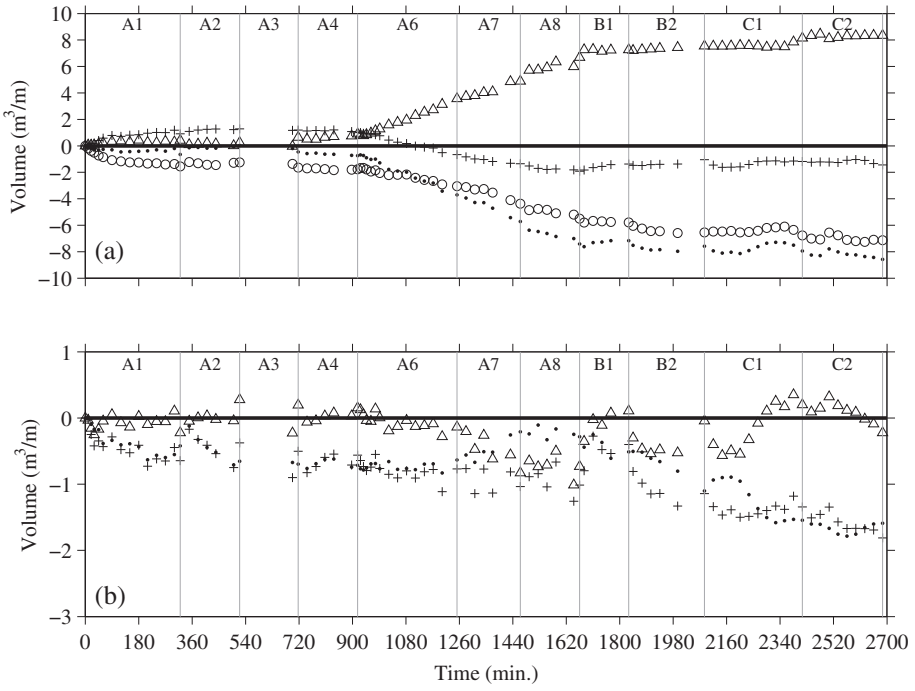

Fig. 4. (a) Volumes V with respect to volume in the initial profile versus time t for (dots) sandbar-trough and (triangles) berm zones ($V_{bt}(t)$ and $V_{berm}(t)$, respectively). The pluses and circles separate the sandbar-trough zone into volumes for the sandbar and trough zones, $V_{bar}(t)$ and $V_{trough}(t)$, respectively. (b) As (a), but now for the (dots) offshore zone, (triangles) sandbar-trough and berm zones combined and (pluses) all three zones combined ($V_{off}(t)$, $V_{bt}(t) + V_{berm}(t)$, and $V_{off}(t) + V_{bt}(t) + V_{berm}(t)$, respectively). Note the different values on the y -axes.

position of $x \approx 72$ m. The trough region and the berm remained largely unaltered until the end of B1. The lowering of the sea level to $h_s = 2.5$ m caused Q_b to increase to 40–60% over the sandbar region and, as a consequence, sediment transports became offshore directed (Fig. 5b) and the sandbar moved offshore by 5 m during the 255-minute long test B2 (Fig. 5a). For most of series C, the water level over the sandbar was too high to cause substantial wave breaking and the sandbar slowly migrated onshore (Fig. 5d–f). Only during the lowest stages of the tide, the sandbar moved offshore but the wave tests were of insufficient duration (30 minutes) to cause major changes. Toward high tide (C1 → C2) wave

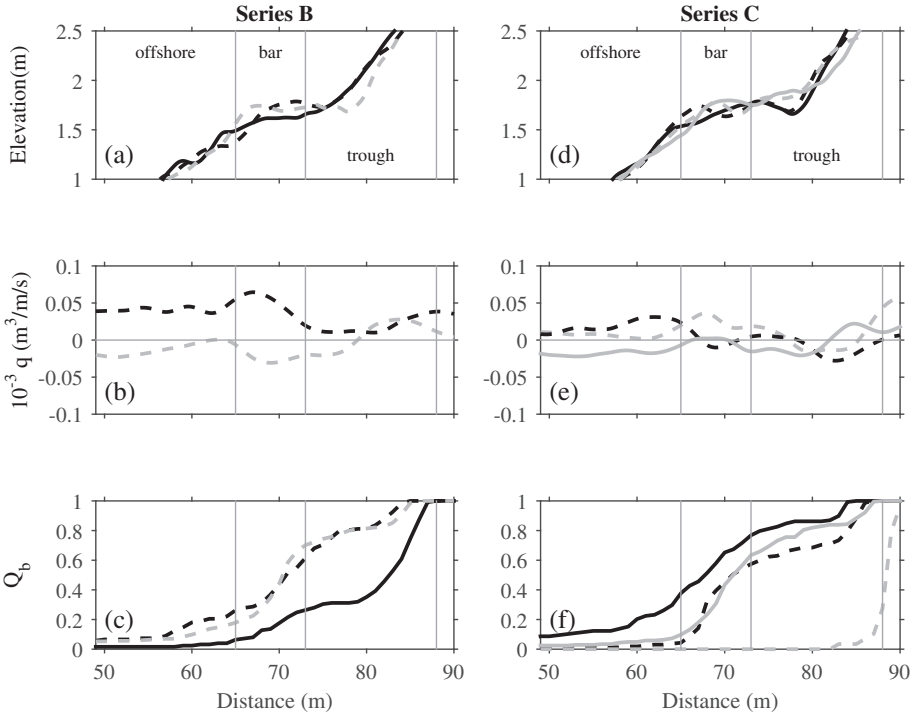

Fig. 5. (Top to bottom) Bed elevation z_{bb}, volumetric transport rate q and fraction of breaking waves Q_b versus cross-shore distance x for (left column) series B and (right column) series C. In (a) and (c) the solid black line is time $t = 1665$ (start B1), the dashed black line $t = 1830$ min (end B1) and the dashed gray line $t = 2085$ min (end B2). In (b), the dashed black line is q with the profiles at $t = 1665$ and 1830 min (i.e., B1) and the dashed gray line with $t = 1830$ and 2085 min (i.e., B2). In (d)–(f) the order of the lines is the same as in Fig. 2, but now with $t = 2115$ (C1), 2265 (C1), 2415 (end of C1) and 2595 min (C2).

run-up occasionally overtopped the berm, causing its volume to increase by approximately 1 m ^{3}/m, see Fig. 4a. The trough region lost about the same amount of sand, suggesting the lower beach face to be the source of the sediment. When viewed over all tests (A1–C2), the total volume (i.e., $V_{off} + V_{bt} + V_{berm}$) varied slightly with time (Fig. 4b), which has also been seen in other laboratory experiments (e.g., Grasso et al., 2011).

3.2. Swash-zone dynamics

3.2.1. Intra-run bed elevation change

Test A2 (Fig. 6a and b) is characterized by overall erosion of up to 60 mm in the lower swash between the SWL and approximately $x = 94$ m. Gradual, minor accretion of up to 20 mm is evident in the upper swash between $x = 96$ m and the runup limit at $x = 102.9$ m. The majority of the bed lowering in the lower swash occurred quickly between 1450 and 1540 s from the start of the series. A closer analysis of the measured bed/swash elevation time series during this period indicates that the majority of bed lowering occurred due to two large swash events which both ran up beyond $x = 102.2$ m and represent two of the eight largest runup events measured during A2. These events caused the bed at $x = 89.4$ m to lower by 53 mm and 30 mm, respectively, and as such were of a comparable scale to the total bed elevation change of −50.9 mm measured at this cross-shore location over the entirety of A2. Following these events, a period of gradual accretion is observed between 1540 and 6700 s. This period of accretion is characterized by numerous small (< 1 mm) positive and negative changes in bed elevation with a slight skewness toward accretion events. After 6700 s, gradual net erosion occurs in the lower swash and bed elevation change is characterized by a slight negative skewness toward erosion events; however, it is noted that this gradual net erosion is interrupted between 8700 and 8900 s during which there is rapid erosion, associated predominantly with 3 swash events which again have relatively large runup excursions to landward of $x = 101.4$ m. Following this period, there is a short period of accretion to bring the bed elevation back up to the level prior to these events, after which the general erosive trend continues at a similar rate. An examination of bed elevation changes at $x = 89.4$ m indicated that although a large runup excursion will not always cause significant bed elevation change in the lower swash, the larger erosive events do tend to be associated with large runup.

Fig. 5c and d shows the morphology changes measured above the SWL during test A4. It is noted that no ultrasonic altimeter data were available for the fourth wave run of A4 (henceforth termed A4_04)

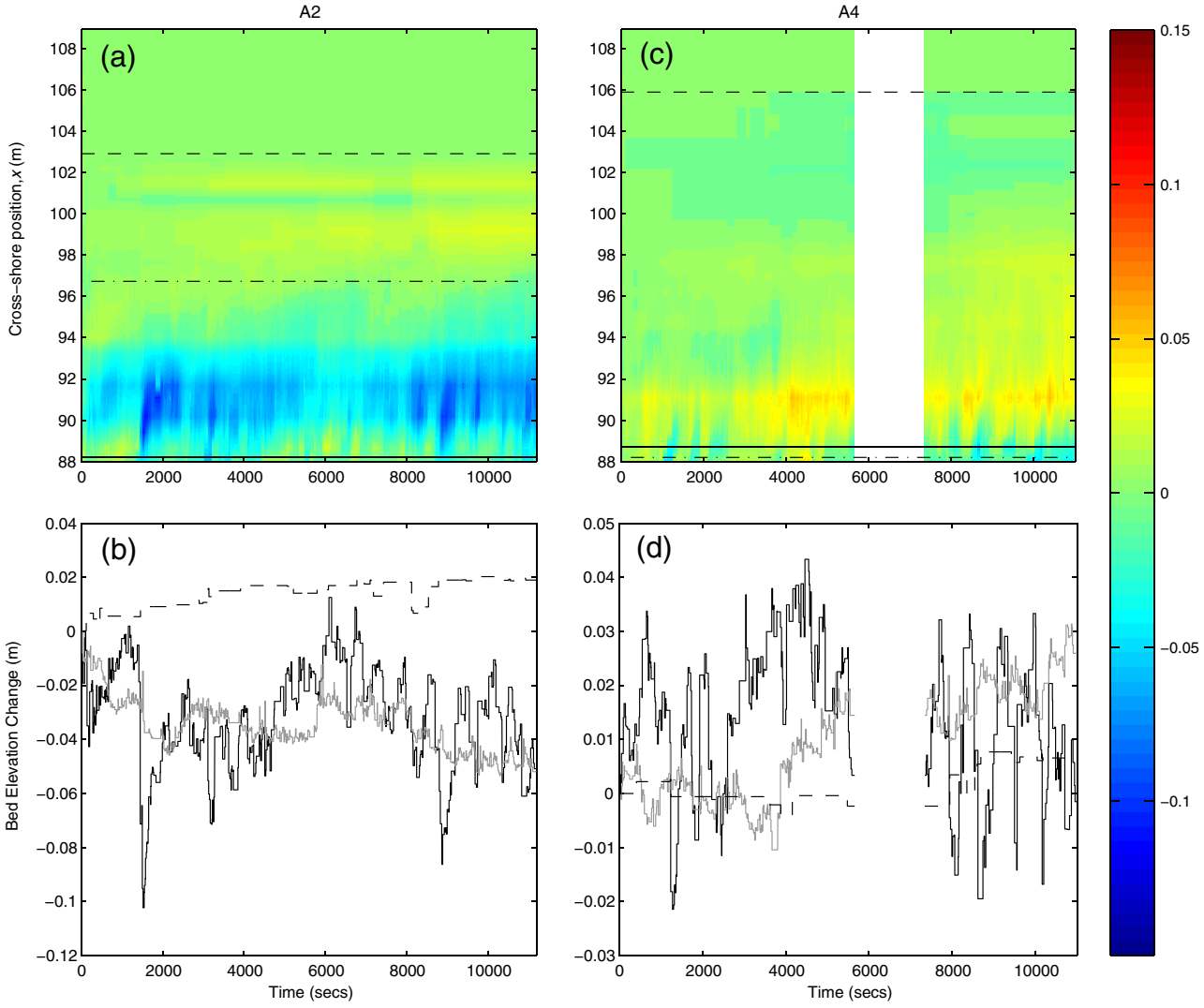

Fig. 6. (Top panels) Change in bed elevation (in m) relative to initial state throughout the beach face for tests (a) A2 and (c) A4. Horizontal dashed lines indicate the cross-shore position of the maximum runup, horizontal solid lines denote the SWL and the dot-dashed line indicates the mean level of the water table during each test. (Lower panels) Time series of bed elevation change relative to the initial state at altimeter positions at the SWL (black), mid swash defined as 1/3 of the swash zone width above SWL (gray) and upper swash defined as 2/3 of the swash zone width above SWL for tests (b) A2 and (d) A4. The white section in (c) and (d) is where no data were available.

and this is indicated by the white section in Fig. 6c and d; however, the measurements suggest that net bed elevation change was minimal during this run. Overall accretion across the whole beach face profile, which was strongest 3 m landward of the SWL (at $x = 91.1$ m), was observed. In contrast to A2, which saw erosion in the lower swash, accretion of up to 40 mm occurred in the lower swash during A4 as a result of rapid fluctuations in bed elevation with periods of rapid accretion and erosion evident in Fig. 6c. Accretion of approximately 10–30 mm in the upper swash between $x = 96$ m to $x = 102.9$ m was similar to A2.

The time series of bed elevation changes during test A7 show evidence of gradual accretion across the whole profile (Fig. 7a and b), with the strongest accretion at the location of the berm crest ($x = 97.5$ m, see Fig. 3e–f), leading to a gradual increase in the crest height and further development of the berm profile. A series of monochromatic waves that were run between runs A7_03 and A7_04 caused significant accretion in the lower swash and some erosion in the upper swash, which can be observed at 5510 s. This run put the beach out of equilibrium with the irregular wave test conditions for run A7_04 and as such, following resumption of the irregular wave runs, there is evidence of fairly rapid bed lowering in the lower swash between 5500 and 6000 s. A similar pattern of gradual accretion in the mid and upper swash to that during A7 is observed during A8 (Fig. 7c and d). The berm continues to increase in height but develops a negative slope on the landward side, into which swashes start to overtop. In the lower swash ($x = 89.4$ m to $x = 94$ m), however, there is little change for the majority of the series until a period of rapid erosion at 9250 s. This erosion was caused by a series of large runup events that overtopped the berm.

Comparing the response observed during tests A2 and A4 when the initial beach face morphology was relatively similar and there was no strong berm feature, a clear difference in the beach response in the lower swash region is observed. During A2, there was erosion of up to 0.11 m in the lower swash, while during A4, accretion of up to 0.06 m was recorded. As the wave conditions during these tests were identical and the initial beach profiles were relatively similar, it is reasonable to assume that while the morphological change was primarily driven by swash processes the lagoon levels had an influence on the morphological response and the overall seaward groundwater gradient during A2 tended to promote erosion in the lower swash, while the landward groundwater gradient during A4 induced accretion. Turner et al.

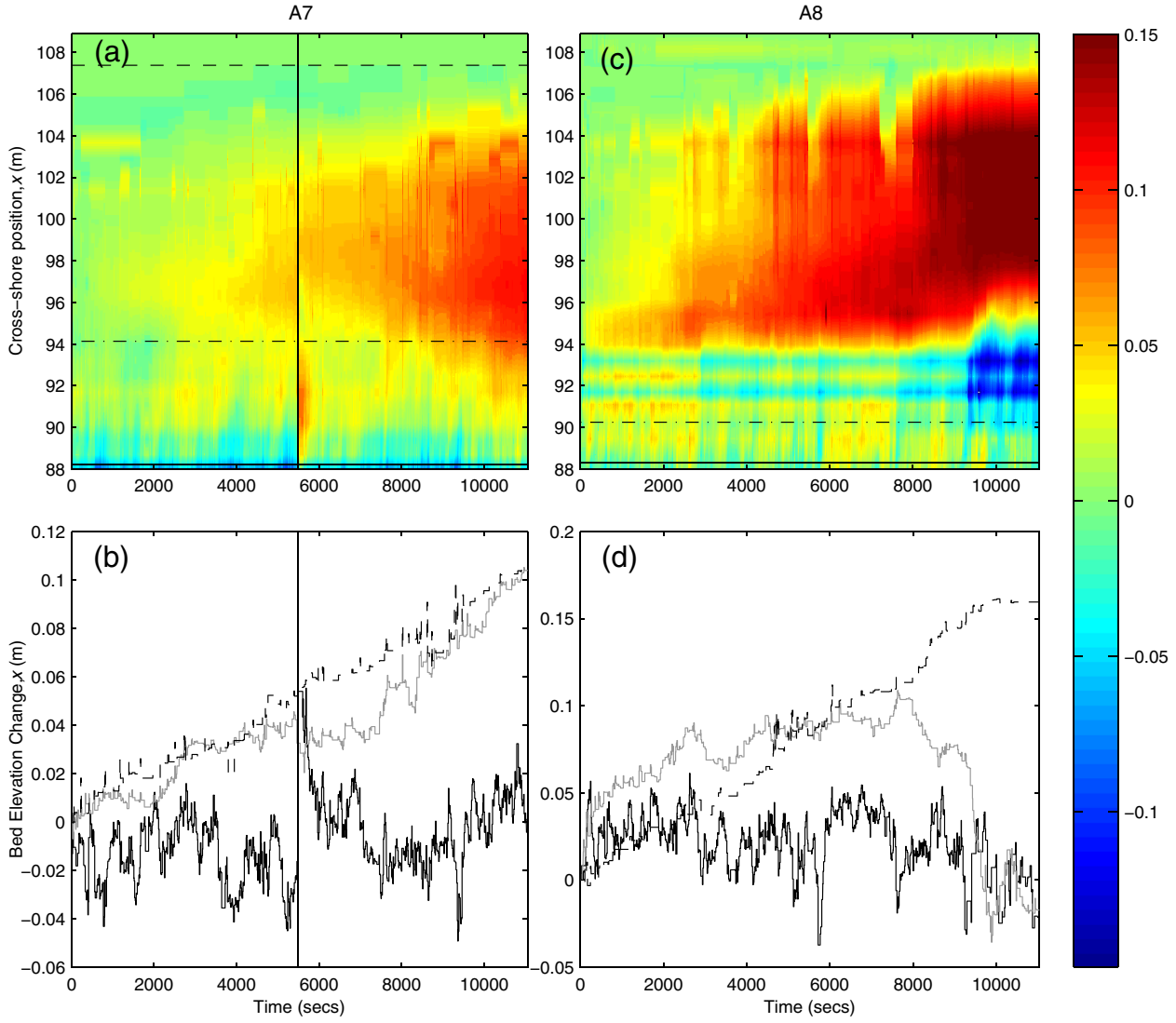

Fig. 7. (Top panels) Change in bed elevation (in m) relative to initial state throughout the beach face for tests (a) A7 and (c) A8. Horizontal dashed lines indicate the cross-shore position of the maximum runup (landward of 108.6 m in A8 and so not shown), horizontal solid lines denote the SWL and the dot-dashed line indicates the mean level of the water table during each test. (Lower panels) Time series of bed elevation change relative to the initial state at altimeter positions at the SWL (black), mid swash defined as 1/3 of the swash zone width above SWL (gray) and upper swash defined as 2/3 of the swash zone width above SWL for tests (b) A7 and (d) A8. The white section in (c) and (d) is where no data were available. The vertical line in (a) and (b) indicates the timing of a short monochromatic wave test which was unrelated to A7 but caused morphology change.

(2016) have undertaken a comprehensive study of groundwater fluxes and flow paths within the barrier for tests A2 and A4 and found that during periods of wave action, a groundwater mound developed at the beach face and this had a comparable profile at both high and low lagoon levels with a similar water table exit point. Despite these similarities, the overall seaward groundwater gradient during A2 led to a net exfiltration rate through the lower beach face an order of magnitude larger than during test A4 (1.4×10^{-6} m/s versus 4.4×10^{-7} m/s, respectively). Numerous authors have examined the effect of seepage flows on sediment stability and have found that exfiltration reduces the effective weight of the surficial sediment particles while also decreasing the shear stress exerted on the particle due to boundary layer thickening (e.g., Nielsen, 1998; Turner and Masselink, 1998; Butt et al., 2001). Discussion remains on the net influence of these effects on sediment stability; however, these studies indicate that for $D_{50} < 400 - 600$ μm, the destabilizing effect of the reduction in effective weight is more important than the stabilizing effect of the boundary layer modification. Thus, for the present study ($D_{50} = 430$ μm) it is hypothesized that the larger net exfiltration rate during test A2 contributes to the observed enhanced erosion on the lower beach face.

The influence of the groundwater gradient during tests A7 and A8 is less evident due to the presence of a strong berm feature that has a significant effect on the morphological response. Wave runup excursions were greater than during tests A2 and A4, and as a consequence the berm feature was regularly overtopped during tests A7 and A8. Due to the localized lowering of the beach gradient on the landward side of the berm, flow reversal of the overtopping water volume was much slower than below the berm crest and the water tended to be held on the slope for a relatively long period in this region. This had the effect of reducing the volume flux of water during backwash and hence reducing the capacity of the backwash to remove sediment from the upper beach face and transport it seawards. This effect was stronger during test A8 due in part to the more defined berm but potentially also because infiltration of water into the beach face would have further reduced the volume flux of water during the backwash. As a consequence, during test A8 sediment was transported from the lower swash region to the berm leading to accretion of the upper swash and a loss of mass in the lower swash zone.

3.2.2. Per event bed elevation changes and volume fluxes

An examination of the per-event bed elevation changes and volume fluxes at each sensor location indicated that both bed level change and volume flux were approximately symmetrically distributed around zero, with skewness values consistently close to zero at all cross-shore locations. A similar result was previously observed in the field by Blenkinsopp et al. (2011). This observed balance between erosive and accretionary swashes restricts net morphology change above SWL, which is consistently an order of magnitude smaller than the cumulative change recorded during each test (see Table 2). The cumulative volume flux per second above the SWL is relatively consistent for the low energy wave condition cases (A2 and A4) and high energy conditions (A7 and A8) but the rate is much larger for the high energy cases (see Table 2). This result indicates that a larger bulk amount of sediment is being transported during energetic wave conditions and this, combined with stronger morphological feedback from the berm feature, leads to a greater net morphology change. It is hypothesized that more energetic waves will consistently move more sand and hence generate a greater cumulative volume flux, but that positive and negative changes will tend to cancel out and the net effect of this transport will be regulated by morphological feedback, controlled by the disequilibrium between the morphological state of the beach and the wave conditions.

Accretion and erosion in the different regions of the swash zone can be explained in terms of the proportion of positive and negative bed elevation changes and volume fluxes (Fig. 8a and b) and the mean per-event positive and negative bed elevation and volume fluxes (Fig. 8c to f). In general terms, Fig. 8a and b shows that there are a slightly greater number of negative per-event bed elevation changes and volume fluxes in the lower part of the swash zone ($x \approx 88.0$ m to 96.0 m) while in the upper swash, the majority of values are positive, though considerable scatter is noted for test A4 due to the small number of swashes with excursions beyond 100.0 m. Fig. 8c and e indicates that the mean positive and negative bed elevation changes at all locations vary in a comparable manner in the cross-shore for each test. Fig. 8d and f demonstrates a similar cross-shore variation in the positive and negative mean per event volume flux values; however, it is noted that the mean positive values are larger in tests A7 and A8, leading to significant net onshore transport and the strengthening of a berm feature (Fig. 3). While the patterns observed in Fig. 8a to f are generally consistent within each test, small differences lead to the net morphological changes observed in Figs. 6 and 7.

In more detail, the mean positive and negative bed elevation changes in the lower swash (taken seaward of $x = 96.0$ m) for tests A2 and A8 are similar, leading to overall mean per event bed elevation changes of + 0.14 mm and + 0.18 mm, respectively. Consequently, the observed net erosion in this region occurs mainly as a result of the observed imbalance in the number of erosive and accretionary events. In tests A4 and A7 however, net accretion is observed due to the mean positive bed elevation changes being on average 0.56 mm and 0.69 mm greater than the mean negative bed elevation changes for A4 and A7, respectively. Closer examination of the per event bed elevation changes at $x = 89.4$ m (the altimeter landward of SWL) for these tests indicates that while there were more large negative than positive changes greater than ± 20 mm, there were many more medium sized positive bed elevation changes in the range 4 to 11 mm than negative changes in an equivalent range. Data supporting this are not shown here but indicate that net accretion observed is caused by an accumulation of mid-sized positive bed elevation changes. Fig. 8a and b indicates that positive per-event bed elevation changes and volume fluxes dominate in the upper swash ($x = 96.0$ to 109.0 m). This leads to consistent accretion in this region in all tests (see Figs. 6 and 7), which is expected as sediment falls out of suspension during flow reversal, but flow velocity during the initial stages of backwash is insufficient to cause equivalent offshore sediment transport in the upper swash. Fig. 7 shows that the magnitude of accretion was much greater during A7 and A8. This results not only from the larger bulk amount of sediment being transported, but also from feedback with the berm itself: as the berm becomes steeper, swash flows will decelerate more quickly and deposit sediment, further reinforcing the berm. A consistent tendency for net accretion in the upper swash has been observed in the field by Blenkinsopp et al. (2011).

3.2.3. Instantaneous bed level change

Simultaneous measurements at the seaward and middle CCP locations permit determination of instantaneous beach slopes in this region

Table 2
Volume flux statistics.

Test	Duration (s)	Net volume change above SWL (m^3/m)	Cum volume change above SWL (m^3/m)	Max. event volume flux (m^3/m/event)	Cum. volume flux per second above SWL (m^3/m/s)
A2	11,200	−0.22	3.53	0.05	0.00031
A4	9,280	0.26	2.51	−0.08	0.00027
A7	11,035	1.43	9.43	0.10	0.00085
A8	11,040	1.53	11.61	−0.23	0.00105

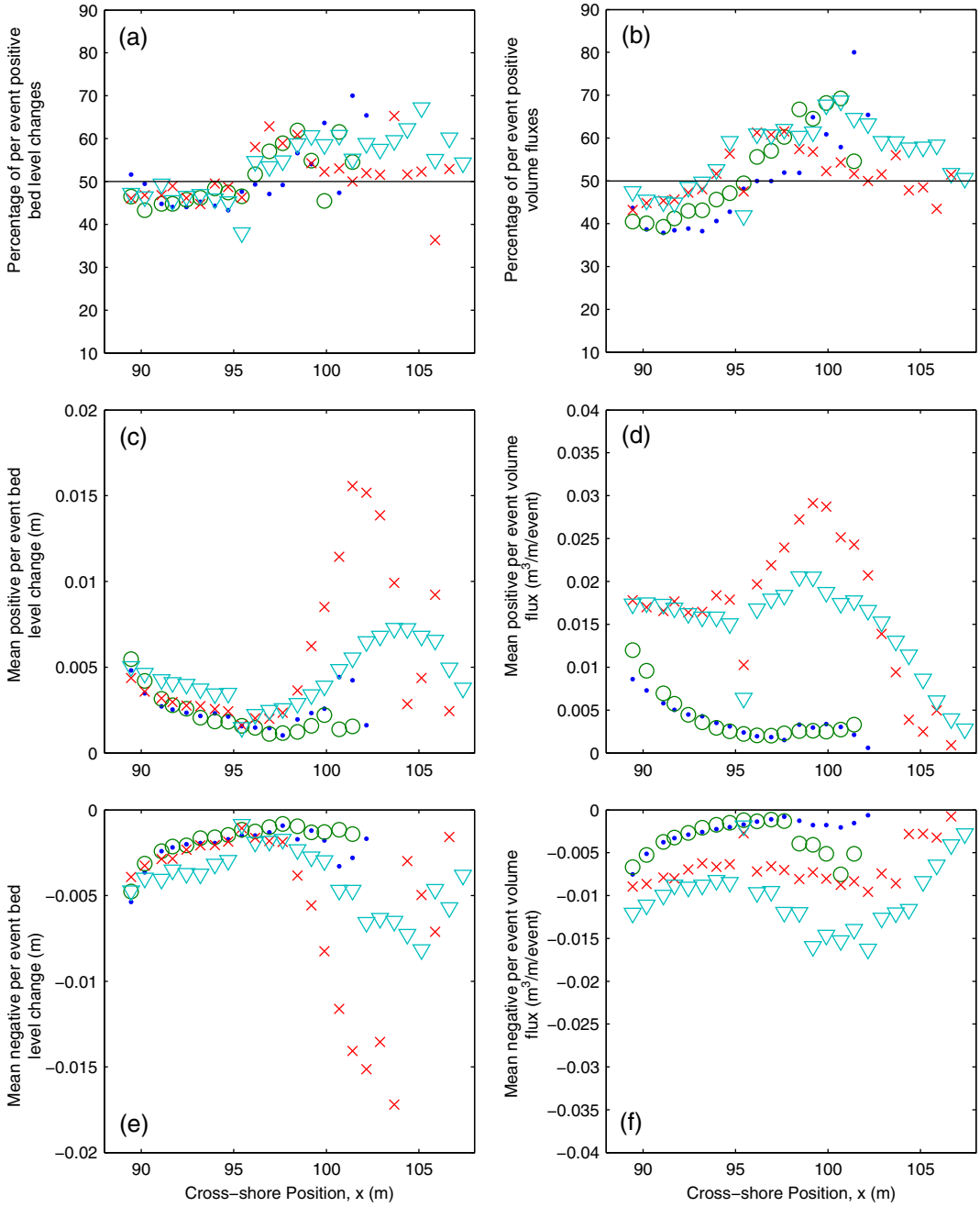

Fig. 8. (a) Percentage of total bed elevation change during events that were positive in magnitude as a function of cross-shore location *x*. (b) Percentage of per event mass flux values that were positive in magnitude. (c) Mean positive per event bed elevation change. (d) Mean positive per event mass flux. (e) Mean negative per event bed elevation change. (f) Mean negative per event mass flux. Blue dots = A2; green circles = A4; red crosses = A7; cyan triangles = A8.

(Fig. 9). The pre (gray) and final (black) profiles for the final irregular wave run for test A2 as recorded by the survey system are also shown. The magenta line shows the median profile from > 20,000 individual estimates of elevation from the cross-shore separated CCP data. The blue lines are the 5 and 95 percentile profiles from the CCP elevation data. The median profile falls within the initial and final beach profile and the percentile profiles encompass the initial and final profiles measured by the survey system. The initial and final measured beach slope determined as a linear fit between the two cross-shore CCP locations for test A2 is 1:10.4 and 1:9.2, respectively. The slope derived from the CCP data for test A2 has a median value of 1:9.2 with 5 and 95 percentiles of 1:8.1 and 1:10.7, respectively. The CCP data indicate that the beach slope can be instantaneously ≈ 25 % steeper or shallower than the median slope from the CCP or initial or final measured slope.

Analysis of the ultrasonic altimeter data at the CCP locations demonstrates that the observed local slope variability is also captured by the altimeters which can measure slope only when the bed is exposed between swash events. Fig. 10 shows that mean slopes and standard deviations obtained from the altimeters are comparable to those obtained by the CCPs, suggesting that the inter- and intra-swash variability is similar between the seaward and central CCP locations. Extending the analysis to incorporate the ultrasonic altimeter data enables the variability of the local slope to be examined across the entire beach face and demonstrates a trend of decreasing mean, maximum and minimum

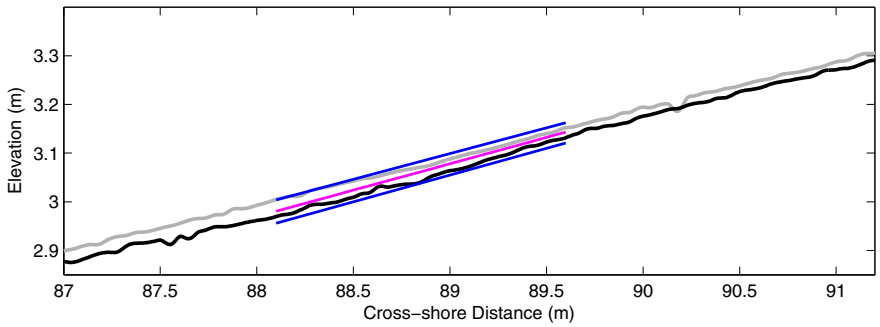

Fig. 9. Initial (gray) and final (black) beach profiles from the last irregular wave run of test A2. Magenta line is the median beach profile from over 20,000 individual foreshore profile segments as determined from cross-shore separated CCP sensors at the seaward and middle locations. Blue lines are the 5th and 95th percentile profiles between the CCP measurements.

slopes in the landward direction for both runs (Fig. 10). Note that during tests A2 and A4 the beach profile was still adjusting from its initial planar slope and as such the beach profile was in a state of transition. In addition, the standard deviation of the local slope is similar for both test cases at all measured locations across the beach face indicating comparable slope variability despite contrasting morphology change as observed in Fig. 6.

The CCP and altimeter data both provide the opportunity to examine bed elevation change at high temporal resolution. However, they both have advantages and disadvantages. The CCPs enable the bed elevation to be captured throughout the swash cycle but have a limited vertical range (0.03 m profiling window). The CCP analysis in this work, thus, focused on the latter 60 minutes of the runs when bed evolution slowed. An effort was made to increase the overall profiling window by deploying multiple sensors offset in the vertical. In some instances this approach was successful but in others it was not. The ultrasonic altimeter data can be used to detect bed elevation change throughout all runs in a test. However, the instrument can only detect the bed when the water depth below the sensor is zero. Thus, the altimeter only 'sees' the bed intermittently in between some swash events. Consequently, the two instruments provide complimentary measurements of the changing bed elevation in the swash zone. The CCPs provide more continuous data in the lower swash zone when the bed is predominantly submerged, while the ultrasonic altimeters provide more complete data in the upper swash zone as the frequency of bed exposure increases.

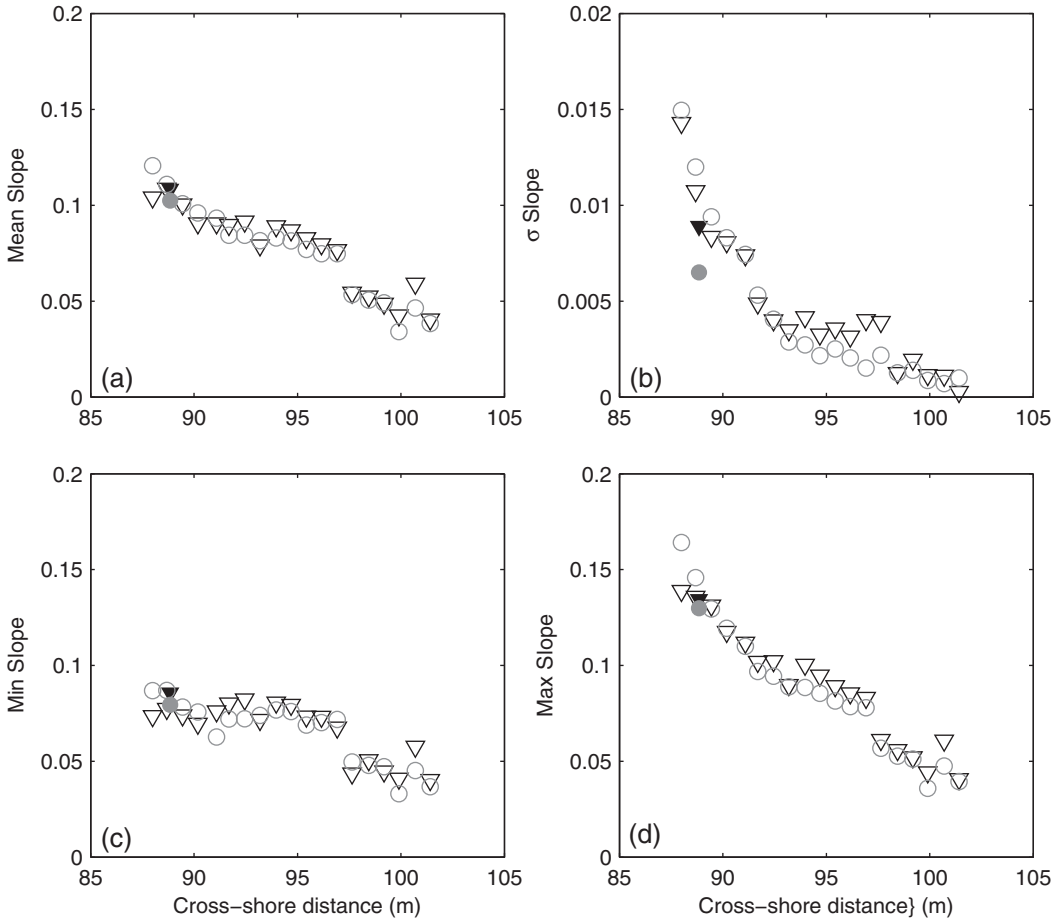

Fig. 10. Cross-shore variation of (a) mean slope, (b) standard deviation in slope, (c) minimum slope and (d) maximum slope for runs A2_05 (triangles) and A4_05 (circles). Open symbols represent values calculated between adjacent ultrasonic altimeters and filled symbols are the values calculated between the seaward and central CCPs.

The rapid fluctuations of local beach slope both within and between swash events have potential implications for numerical modeling of swash zone sediment transport. Locally changing beach slope will influence local flow velocity and also the stability of sediment. Fredsoe and Deigaard (1992) suggest a modification to the Shields parameter to account for the effect of a sloping bed on the initiation of local sediment motion. Dodd et al. (2008) introduced a slope-dependent bed diffusion source term into their model which is updated at every time step. Failure to update beach morphology has been shown in some cases to cause a reduction in the ability of models to accurately predict hydrodynamics and hence sediment transport over model runs of many minutes (e.g., Ruessink, 2005; McCall et al., 2014). The existence of such rapid, local morphological variability as observed in the present measurements suggests that it may be beneficial to update morphology at the wave-by-wave timescale or even greater and highlights the benefits of implementing a fully-coupled approach to modeling hydrodynamics, sediment transport and morphological evolution (e.g., Zhu and Dodd, 2015).

4. Sandbar modeling

While the net cross-shore volumetric transport rate can be inferred from the bed profile data set $z_{bb}(x, t)$, this provides no insight into which sand-transport processes contributed to this net rate. In this section we will rely on numerical modeling to examine the role of individual processes. The model deployed, described in Dubarbier et al. (2015b), is a phase-averaged model that contains fully coupled modules for waves, currents, sand transport and bed-level change. It was chosen because velocity skewness and asymmetry, mean currents and gravity all contribute to sand transport. Other models, like Plant et al. (2004) and Ruessink et al. (2007), typically ignore the role of velocity asymmetry. The model's wave, current and bed-level change modules are largely similar to those in Ruessink et al. (2007). The sand transport module follows the energetics approach of Hsu et al. (2006), with the addition of transport by wave asymmetry proposed by Hoefel and Elgar (2003). Input for the transport module are the near-bed mean current and the skewed-asymmetric shape of the near-bed, free-stream wave orbital motion based on the approach of Ruessink et al. (2012). In this approach, the local root-mean-square wave height, peak period and water depth are combined into the Ursell number and related to near-bed velocity skewness S_u and asymmetry A_u through fits based on several field data sets. Ruessink et al. (2012) argued that their prediction of in particular S_u might not be suitable for unidirectional (i.e., laboratory) swell conditions, as is the case here. Values of S_u measured along the flume revealed (not shown) that the overall dependence of S_u on the Ursell number was the same as observed in the field data sets, but that in the flume the maximum S_u was larger ($\approx$ 1.0 versus 0.6) and the decline in S_u for large Ursell numbers (i.e., in the inner surf zone) was less pronounced. To accommodate for these observations, the functional S_u fit proposed by Ruessink et al. (2012) was retained, but its free parameters were adjusted to better match the BARDEX II observations (see Dubarbier et al., 2015a). The fit for A_u was not altered. With the wave height and period, and water level measured at $x = 49$ m as input, the free parameters in the sand transport module were calibrated to minimize the squared difference between observed and predicted bed profiles ($x = 60 - 90$ m) of series C with the simulated annealing algorithm outlined in Dubarbier et al. (2015b). Series C was chosen for calibration because it contains both onshore and offshore sandbar migration (Fig. 5). The optimized values were, without additional calibration, applied in test A1, in which the sandbar formed from the initially planar profile (Fig. 3). The model does not incorporate swash processes and can, accordingly, not be used to simulate berm formation (tests A6–A8).

As can be seen in Fig. 11a–b, the optimized model was capable of reshaping the initially planar beach into a barred profile during test A1. However, the rate of sandbar formation was substantially underpredicted. While at $t = 90$ min the sandbar was already observed to be almost in equilibrium with the wave conditions (Section 3.1), the modeled sandbar just resembled the measured sandbar (in terms of volume) at the end of the simulation ($t = 300$ min, Fig. 11b). In more detail, the sandbar was then predicted to be wider and less pronounced than in the observations; also the trough ($x > 73$ m) did not form. The slower formation of the sandbar is also reflected in the model skill, estimated here as a Brier Skill score (e.g., Sutherland et al., 2004) using a no-change model as reference. In this way, model skill equals 1 in case of perfect agreement with the observations, 0 when the model performance is equal to a no-change model, and negative when applying no-change would actually have been better than running the model. Here, the skill was close to 0 for the first 60 min, reflecting the slow initial formation of the sandbar, and increased to 0.75 later on in the simulation when the predicted sandbar started to resemble the observed sandbar. In series C, the model reproduced the temporal change from offshore to onshore and back to offshore migration with tidal level, although the onshore migration of the seaward edge of the terraced

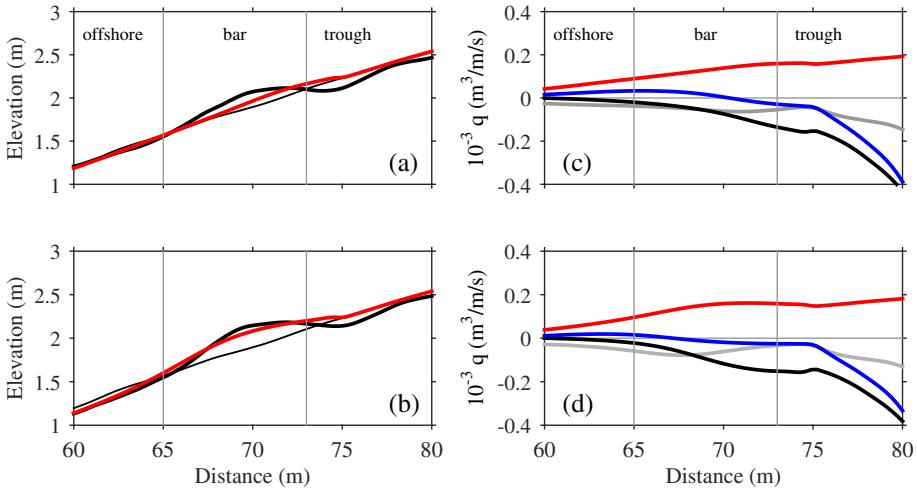

Fig. 11. Simulation of test A1 with the optimized (i.e., based on series C) free parameters and the new parameterization for wave skewness S_u. (a)–(b) show the predicted (red) and observed (black) bed profiles at $t = 90$ and 300 minutes, respectively. The thin sloping line in each panel is the initial planar profile. (c)–(d) show the transport rates induced by velocity asymmetry (red), cross-shore mean flow (black) and gravity (gray) versus cross-shore distance x at $t = 90$ and 300 minutes, respectively. The net transport rate is shown in blue in both panels.

sandbar was clearly underestimated, see also Dubarbier et al. (2013). By the end of this simulation, model skill amounted to about 0.8, implying that the model performed clearly better than a no-change model. As expected, the model did not perform well in the swash zone, which, although not shown in Fig. 11a–b, can be inferred from the unrealistic increase in net transport rates for ($x > 75$ m; Fig. 11c–d, compare to Fig. 3c). Because our simulations were rather short (hours), it seems unlikely that these strong negative transport rates already affected the evolution of the terraced bar further seaward. Earlier simulations with a similar model (Ruessink, 2005) illustrated that unrealistic beach face evolution can lead to the disappearance of the bar-trough and hence affect bar dynamics after several storms (weeks). In other words, the lack of shoreline processes is not problematic for realistic beach face predictions only but it can eventually lead to a degradation in model performance in the surf zone too.

Fig. 11c–d illustrates the predicted sand transport rates by velocity asymmetry, cross-shore mean flow and gravity, as well as the total (net) transport, at $t = 90$ and 300 min in test A1. Values for the transport rates by velocity skewness were near-zero throughout and are not shown for clarity. Consistent with the observations (Fig. 3c), the model predicted near-zero net transport rates in the offshore zone ($x < 65$ m). The model suggests that these near-zero values are due to a near-balance between onshore transport by velocity asymmetry and offshore transport by a mean flow (the undertow) and gravity. Thus, our inference that the sandbar formed in response to gradients in the offshore directed transport rather than to convergence of onshore and offshore transport (Fig. 3c) should not be interpreted as that sand transport by wave non-linearity is unimportant. Instead, the transport by wave asymmetry largely opposes that by the undertow and thus strongly affects the magnitude and gradient of the net transport. In contrast to earlier simulations on substantially more gentle bed profiles (e.g., Ruessink et al., 2007; Dubarbier et al., 2015b), the downslope gravity-induced transport is not negligible on the present steep slope. In the sandbar zone the predicted net transport rate became slightly negative because the undertow-related transport rates increase more rapidly in magnitude than the velocity-asymmetry induced transport rate. The inability of the model to handle shoreline processes is obvious from predicted transport rates at $x > 75$ m. Here, in sharp contrast to the observations in Fig. 3c, the net transport rate becomes strongly more negative, while in the observations the net rates become positive to result in a small berm. Consistent with field observations (e.g., Gallagher et al., 1998) and other numerical model predictions (e.g., Plant et al., 2004; Ruessink et al., 2007; Walstra et al., 2012; Kuriyama, 2012), the offshore sandbar migration in series C was predicted to be due to gradients in the undertow-related transport, although the magnitude of this transport term was strongly counteracted by the onshore transport by velocity asymmetry. During the higher stages of the tide, the transport rates by the mean current and the velocity asymmetry both diminished and velocity skewness became the largest contributor to the net transport rate. Additional simulations (e.g., Dubarbier et al., 2013) indicate that the inclusion of velocity asymmetry is crucial to overall positive skill in series C; without this term, the model would have overestimated offshore sandbar migration, and underestimated onshore sandbar migration even more.

5. Conclusions

We examined bed level change on a near-prototype, initially steep (1:15) and planar, coarse-grained ($D_{50} = 430$ μm) barrier in response to different wave conditions, and sea and lagoon water levels. We distinguished between sandbar and berm dynamics (including, surf–swash sand exchange; time scale of tens of minutes to hours), the net effect of single and multiple swash events on the entire beach face (time scale of a few seconds to hours), and instantaneous bed variability at 3 cross-shore locations within individual swashes. During high-energy waves ($H_s = 0.8$ m, $T_p = 8$ s) sand was predominantly eroded from the inner surf zone, just below the still water level (SWL), to be deposited in the outer surf zone as a sandbar, and on the beach face as a small berm. Based on numerical simulations with a process-based morphodynamic model, velocity asymmetry, undertow and gravity are all suggested to be important to this sandbar formation. In the lower swash zone, sand was deposited when the ground water gradient in the barrier was landward (low lagoon levels) and was eroded under a seaward gradient (high lagoon levels). Subsequent low-energy, high-period waves ($H_s = 0.6$ m, $T_p = 12$ s) caused substantially larger surf–swash sand exchange: the pre-existing sandbar migrated onshore and decayed, with the sand ending up on the beach face in a prominent (up to 0.7 m high), steep (1:6) berm. Following this, the effects of lagoon level on beach face dynamics were negligible; instead, the berm grew more quickly by decelerating swash flows, forcing sediment deposition and further berm growth. Thus, we found berm dynamics to be governed by wave conditions and the antecedent morphology, with ground water gradients of additional importance when morphodynamic feedback between swash flow and the berm is small. Consistent with earlier field observations, bed level change within a swash and averaged over a swash event could be substantial (several centimeters) during all wave conditions, but the net (i.e., averaged over multiple swash events) bed level change was strongly suppressed because erosive and accretionary swashes nearly balanced. In addition, the local beach face slope could be instantaneously ≈ 25 % steeper or shallower than the median slope, or the initial or final slope. Tidal variations in sea water level forced temporal variability in the direction of sandbar migration, with onshore migration when less than some 20% of the waves broke at the sandbar and offshore migration when breaking was more intense. Berm growth was now restricted to overtopping during the highest water levels.

Acknowledgments

The work described here was supported by the European Community's 7th Framework Programme through the grant to the budget of the Integrating Activity HYDRALAB IV, contract no. 261520. The academic lead of the project was Gerd Masselink and the Deltares coordinator was Guido Wolters. We would like to thank the Delta Flume staff (Leen, Johan, Piet and Ab) for making the experiment such an enjoyable and successful experience. GR and JB were additionally funded by the Dutch Technology Foundation STW, which is part of the Netherlands Organisation for Scientific Research (NWO), and which is partly funded by the Ministry of Economic Affairs (project number 12397). JP and TL were funded by the National Science Foundation (NSF; OCE-0845004) and the University of Delaware. JP was additionally funded by the US/UK Fulbright commission and NSF (OCE-13322703). BD and BC received financial support from the French National Research Agency through projects BARBEC (ANR-N2010-JCJC-602-01) and CHIPO (ANR-14-ASTR-0004-01). Additional support for CB was provided by an Australian Research Council Discovery Grant (DP110101176).

References

Archie, G.E., 1942. The electrical resistivity log as an aid in determining some reservoir characteristics. Pet. Trans. AIME 146, 54–62.
Aubrey, D.G., 1979. Seasonal patterns of onshore/offshore sediment movement. J. Geophys. Res. 84, 6347–6354.
Bagnold, R.A., 1966. The shearing and dilatation of dry sand and the 'singing' mechanism. Philos. Trans. R. Soc. London, Ser. A 295, 219–232.
Blenkinsopp, C.E., Turner, I.L., Masselink, G., Russell, P.E., 2011. Swash zone sediment fluxes: field observations. Coast. Eng. 58, 28–44.
Brinkkemper, J.A., Lanckriet, T., Grasso, F., Puleo, J.A., Ruessink, B.G., 2016. Observations of turbulence within the surf and swash zones of a field-scale sandy laboratory beach. Coast. Eng. 113, 62–72.
Butt, T., Russell, P., Turner, I., 2001. The influence of swash infiltration-exfiltration on beach face sediment transport: onshore or offshore? Coast. Eng. 42, 35–52.
Dodd, N., Stoker, A., Calvete, D., Sriariyawat, A., 2008. On the evolution of beach cusps. J. Fluid Mech. 597, 145–169.
Dubarbier, B., Castelle, B., Marieu, V., Ruessink, G., 2013. Numerical modelling of pronounced sloping beach profile evolution: comparison with the large-scale BARDEX II

experiment. In: Conley, D.C., Masselink, G., Russell, P.E., O'Hare, T.J. (Eds.), Proceedings 12th International Coastal Symposium (Plymouth, England). Journal of Coastal Research 65, pp. 1762–1767.
Dubarbier, B., Castelle, B., Marieu, V., Ruessink, B.G., 2015a. On the modeling of sandbar formation over a steep beach profile during the large-scale wave flume experiment BARDEX II. In: Wang, P., Rosati, J.D., Cheng, J. (Eds.), Proceedings Coastal Sediments 2015. World Scientific.
Dubarbier, B., Castelle, B., Marieu, V., Ruessink, G., 2015b. Process-based modelling of cross-shore sandbar behaviour. Coast. Eng. 95, 35–50.
Fredsoe, J., Deigaard, R., 1992. Mechanics Of Coastal Sediment Transport. World Scientific, Singapore.
Gallagher, E.L., Elgar, S., Guza, R.T., 1998. Observations of sand bar evolution on a natural beach. J. Geophys. Res. 103, 3203–3215.
Grasso, F., Michallet, H., Barthelemy, E., 2011. Experimental simulation of shoreface nourishments under storm events: a morphological, hydrodynamic, and sediment grain size analysis. Coast. Eng. 58, 184–193.
Grunnet, N.M., Walstra, D.J.R., Ruessink, B.G., 2004. Process-based modelling of a shoreface nourishment. Coast. Eng. 51, 581–607.
Hamm, L., Capobianco, M., Dette, H.H., Lechuga, A., Spanhoff, R., Stive, M.J.F., 2002. A summary of European experience with shore nourishments. Coast. Eng. 47, 237–265.
Hoefel, F., Elgar, S., 2003. Wave-induced sediment transport and sandbar migration. Science 299, 1885–1887.
Holman, R.A., 2000. Pattern formation in the nearshore. In: Seminara, G., Blondeaux, P. (Eds.), River, Coastal And Estuarine Morphodynamics. Springer Verlag, Berlin, pp. 141–162.
Holman, R.A., Stanley, J., 2007. The history and technical capabilities of Argus. Coast. Eng. 54, 477–491.
Hsu, T.J., Elgar, S., Guza, R.T., 2006. Wave-induced sediment transport and onshore sandbar migration. Coast. Eng. 53, 817–824.
Kobayashi, N., Jung, H., 2012. Beach erosion and recovery. J. Waterw. Port Coast. Ocean Eng. 138, 473–483.
Kuriyama, Y., 2012. Process-based one-dimensional model for cyclic longshore bar evolution. Coast. Eng. 62 (48-16).
Lanckriet, T., Puleo, J.A., Waite, N., 2013. A conductivity concentration profiler for sheet flow sediment transport. IEEE J. Ocean. Eng. 38, 55–70.
Lanckriet, T., Puleo, J., Masselink, G., Turner, I., Conley, D., Blenkinsopp, C., Russell, P., 2014. Comprehensive field study of swash-zone processes. II. Sheet flow sediment concentrations during quasi-steady backwash. J. Waterw. Port Coast. Ocean Eng. 140, 29–42.
Masselink, G., Ruju, A., Conley, D., Turner, I., Ruessink, G., Matias, A., Thompson, C., Castelle, B., Puleo, J., Citerone, V., Wolters, G., 2016. Large-scale Barrier Dynamics Experiment II (BARDEX II): experimental design, instrumentation, test programme, and data set. Coast. Eng. 113, 3–18.
Matias, A., Masselink, G., Castelle, B., Blenkinsopp, C., Kroon, A., 2016. Measurements of morphodynamic and hydrodynamic overwash processes in a large-scale wave flume. Coast. Eng. 113, 33–46.
McCall, R.T., Masselink, G., Poate, T.G., Roelvink, J.A., Almeida, L.P., Davidson, M., Russell, P.E., 2014. Modelling storm hydrodynamics on gravel beaches with XBeach-G. Coast. Eng. 91, 231–250.
Nielsen, P., 1998. Coastal groundwater dynamics. Proceedings Coastal Dynamics. ASCE, pp. 546–555.
O'Donoghue, T., Wright, S., 2004. Concentrations in oscillatory sheet flow for well sorted and graded sands. Coast. Eng. 50, 117–138.
Pender, D., Karunarathna, H., 2013. A statistical-process based approach for modelling beach profile variability. Coast. Eng. 81, 19–29.
Plant, N.G., Holland, K.T., Puleo, J.A., 2002. Analysis of the scale of errors in nearshore bathymetric data. Mar. Geol. 191, 71–86.
Plant, N.G., Holland, K.T., Puleo, J.A., 2004. Prediction skill of nearshore profile evoluation models. J. Geophys. Res. 109. http://dx.doi.org/10.1029/2003JC001995.
Puleo, J.A., Torres-Freyermuth, A., 2015. The second international workshop on swash-zone processes. Coast. Eng. http://dx.doi.org/10.1016/j.coastaleng.2015.09.007.
Quartel, S., Kroon, A., Ruessink, B.G., 2008. Seasonal accretion and erosion patterns of a microtidal sandy beach. Mar. Geol. 250, 19–33.
Ruessink, B.G., 2005. Predictive uncertainty of a nearshore bed evolution model. Cont. Shelf Res. 25, 1053–1069.
Ruessink, B.G., Houwman, K.T., Hoekstra, P., 1998. The systematic contribution of transporting mechanisms to the cross-shore sediment transport in water depths of 3 to 9 m. Mar. Geol. 152, 295–324.
Ruessink, B.G., Kuriyama, Y., Reniers, A.J.H.M., Roelvink, J.A., Walstra, D.J.R., 2007. Modeling cross-shore sandbar behavior on the timescale of weeks. J. Geophys. Res. 112, F03010. http://dx.doi.org/10.1029/2006JF000730.
Ruessink, B.G., Ramaekers, G., Van Rijn, L.C., 2012. On the parameterization of the free-stream non-linear wave orbital motion in nearshore morphodynamic models. Coast. Eng. 65, 56–63.
Sonu, C.J., 1973. Three-dimensional beach changes. J. Geol. 81, 42–64.
Sutherland, J., Peet, A.H., Soulsby, R.L., 2004. Evaluating the performance of morphological models. Coast. Eng. 51, 917–939.
Turner, I.L., Masselink, G., 1998. Swash infiltration–exfiltration and sediment transport. J. Geophys. Res. 103, 30813–30824.
Turner, I.L., Russell, P.E., Butt, T., 2008. Measurement of wave-by-wave bed-levels in the swash zone. Coast. Eng. 55, 1237–1242.
Turner, I.L., Rau, G.C., Austin, M.J., Andersen, M.S., 2016. Groundwater fluxes and flow paths with coastal barriers: observations from a large scale laboratory experiment (BARDEX II). Coast. Eng. 113, 104–116.
Walstra, D.J.R., Reniers, A.J.H.M., Ranasinghe, R., Roelvink, J.A., Ruessink, B.G., 2012. On bar growth and decay during interannual net offshore migration. Coast. Eng. 60, 190–200.
Weir, F.M., Hughes, M.G., Baldock, T.E., 2006. Beach face and berm morphodynamics fronting a coastal lagoon. Geomorphology 82, 331–346.
Winant, C.D., Inman, D.L., Nordstrom, C.E., 1975. Description of seasonal beach changes using empirical eigenfunctions. J. Geophys. Res. 80, 1979–1986.
Zhu, F., Dodd, N., 2015. The morphodynamics of a swash event on an erodible beach. J. Fluid Mech. 762, 110–140.